Pergamon

Geochimica et Cosmochimica Acta, Vol. 66, No. 8, pp. 1401–1407, 2002

0016-7037/02 $22.00 + .00

PII S0016-7037(00)00858-4

Advances in lithium analysis in solids by means of laser-induced breakdown spectroscopy: An exploratory study

CÉCILE FABRE,[1,*] MARIE-CHRISTINE BOIRON,[1] JEAN DUBESSY,[1] ALIOUKA CHABIRON,[1] BERNARD CHAROY,[2] and TOMAS MARTIN CRESPO[3]

[1]CREGU and UMR G2R 7566, BP23, 54501 Vandoeuvre-lès-Nancy Cedex, France
[2]ENSG and CRPG-CNRS EP 2031, BP20, 54501 Vandoeuvre-lès-Nancy Cedex, France
[3]Facultad de Ciencas Geologicas, Universidad Complutense, 28040 Madrid, Spain

(*Received March* 9, 2001; *accepted in revised form October* 24, 2001)

Abstract—Lithium is an important geochemical tracer for fluids or solids. However, because the electron microprobe cannot detect Li, variations of Li abundance at the micrometric scale are most often estimated from bulk analyses. In this study, the Li intense emission line at 670.706 nm in optical emission spectroscopy was used to perfect the analysis of Li at the micrometric scale by means of laser-induced breakdown spectroscopy (LIBS). To estimate lithium content for different geological materials, LIBS calibration of the emission line at 670.706 nm was achieved by use of synthetic glasses and natural minerals. The detection limit for this method is ~5 ppm Li. Three applications to geological materials show the potential of LIBS for lithium determination, namely for Li-bearing minerals, melt inclusions, quartz, and associated fluid inclusions.

For spodumene and petalite from granite pegmatite dikes (Portugal), the Li_2O concentrations are 7.6 ± 1.6 wt% and 6.3 ± 1.3 wt%, respectively, by use of LIBS. These values agree with ion microprobe analyses, bulk analyses, or both. For eucryptite crystals, the Li concentrations are scattered because grain size is smaller than the LIBS spatial resolution (6 to 8 μm). Lithium concentrations of melt inclusions from the Streltsovka U deposit (Siberia) are in the range of 2 to 6.2 wt% (Li_2O) for Li-rich daughter minerals. Lithium estimations on silicate glasses display values between 90 and 400 ppm.

Lithium was also analyzed as a trace element in quartz. Transverse profiles were performed in hydrothermal barren quartz veins from the Spanish Central System (Sierra de Guadarrama). The highest Li concentrations (250 to 370 ppm) were found in specific growth bands in conjunction with the observed variation in optical cathodoluminescence intensity. Considering the fluid inclusion analysis, the source of fluid responsible to the Li enrichment in quartz is probably high-salinity fluids derived from sedimentary basins.

1. INTRODUCTION

It is well known that trace element data are essential for modeling petrological processes such as partial melting, crystal fractionation, assimilation, or hydrothermal reworking. In particular, small differences in element partitioning within minerals permit the identification of various magmatic processes. For instance, during partial melting or fractionation processes (London, 1992), lithium preferentially partitions into the melt, so Li can be routinely used as a tracer for magmatic processes (Seitz and Woodland, 2000). Lithium is also considered to be an important geochemical tracer for fluids or solids (Henley et al., 1984).

Because lithium cannot be determined by the electron microprobe technique, several alternative methods have been proposed to overcome this analytical deficiency. Most of them are empirical and refer to the concentration of another element (Si, F) in natural Li-rich minerals (Brock, 1974; Stern et al., 1986; Tindle and Webb, 1990; Tischendorf et al., 1997). The intense emissivity of Li in optical emission spectroscopy improves its quantification at the micrometric scale via laser-induced breakdown spectroscopy (LIBS). It thus represents an efficient localized analytical technique on solid and liquid materials (Geertsen et al., 1996; Mauchien et al., 1996; Fabre et al., 1999, 2001; Fabre, 2000).

* Author to whom correspondence should be addressed (cecile.fabre@g2r.uhp-nancy.fr).

This article describes the calibration of the method by using synthetic glasses and minerals and presents three applications to test the potential of LIBS for lithium analysis of geological materials at the micrometric scale. The first study focuses on Li-rich minerals (spodumene, petalite, and eucryptite) in granite pegmatite dikes from Portugal (Charoy et al., 2001). A second study deals with melt inclusions with daughter minerals from Russian uranium deposits. The third application examines hydrothermal quartz veins from the Spanish Central system (Martin Crespo et al., 1999).

2. PRINCIPLES AND EXPERIMENTAL PROCEDURE

2.1. Principle of LIBS

The possible effects of absorption of laser radiation on a material include heating, melting, vaporization, atomization, excitation, and ionization, depending on the energy deposited on the sample. Lines emitted from excited atoms and ions are used in laser microanalysis based on plasma emission spectroscopy (Moenke-Blankenburg, 1989; Radziemski and Cremers, 1989; Geertsen et al., 1996). The incident laser radiation generates high-temperature plasma containing atoms and ions in an excited state. Photons are emitted during the return of atoms and ions from an excited, high level to a lower electronic level.

The intensity of an emission line during such an electronic transition is written (André, 1995)

$$I_{ij} = \frac{\Omega \hbar c N g_i A_{ij}}{4\pi \lambda_{ij} Z(T)} \exp\left(\frac{-E_i}{kT}\right) \quad (1)$$

where I is the intensity of the emission line corresponding to the

transition i → j; i and j are the index of the higher and lower energetic quantum state; Ω is the collection solid angle for the plasma emission; ħ is Planck's constant; c is the speed of light; N is the number of free atoms of the studied element in the plasma; g_i is statistical weight of the quantum state i; A_{ij} is transition probability for spontaneous emission from i to j; λ_{ij} is the wavelength of the emission line; Z (T) is the partition function of the quantum state; T is the electronic excitation temperature (K); and E_i is the energy level of excited electronic level i.

2.2. LIBS Instrument and Operating Conditions

A Nd-YAG laser (266 nm) coupled with an optical emission spectrometer delivers a laser pulse (energy per pulse = 2.6 mJ). The laser beam is focused onto the sample through a Cassegrain-type microscope objective (40 mm working distance), thus generating plasma during the laser–matter interaction. The typical emission lines of the elements present in the plasma are directly analyzed with a spectrometer equipped with a pulsed and gated intensified photodiode array. An adjustable time delay filters the continuous emission occurring in the first tens of nanoseconds after the laser shot and optimizes the signal-to-background noise ratio. The optimal delay is 150 ns for a temporal window of 500 ns. The monochromator has a focal length of 280 nm and is equipped with two gratings with 300 grooves mm^{-1} blazed at 250 and 600 nm, respectively. A 200-nm spectral range is simultaneously recorded, utilizing the 300 grooves mm^{-1} holographic grating. The spectral resolution of the spectrograph is 1.2 nm.

2.3. LIBS Analysis Characteristics

The lateral resolution is ~6 to 8 μm for each type of material, although the depth of the resulting crater hole varies from 1 μm for quartz up to 6 μm for copper. Sweeping the sample with an argon flow enhances the plasma temperature and improves the line intensities (Geertsen et al., 1996). A cell especially adapted to work under a constant argon atmosphere with an optimized argon flux has been designed to obtain the best reproducibility of the signal (0.8 L min^{-1}). LIBS analyses do not require any sample preparation, coating, or vacuum, and the time for an analysis (including laser shot and spectrum acquisition) takes a few seconds.

3. CALIBRATION

3.1. Calibration Standards

The determination of elemental concentration in solids requires the calibration of the method with standards consisting of synthetic glasses, minerals, or both. Synthetic glasses were prepared from carbonates ($CaCO_3$, Na_2CO_3, K_2CO_3) and oxide (Li_2O) in a SiO_2 matrix (Table 1). After decarbonation, powders were placed twice in platinum crucibles in a furnace at ~1300°C for 10 min. Between the two heating runs, glasses were ground to around 1 μm for homogenization. The composition of the synthetic glasses was then analyzed by wet chemical methods. In addition, homogeneous Li minerals (a lepidolite and a muscovite; Table 2) of known compositions (analyzed by inductively coupled plasma Atomic Emission spectroscopy) were used.

3.2. Calibration Curve

The emission spectra were collected in the 580- to 780-nm spectral range covering the main lines of major elements present in the sample (Na, K, Ca, Mg, Si). The net intensity of the Li emission line (670.706 nm; resonance transition $1s^22s \rightarrow 1s^22p$) was used to establish the calibration curve for lithium concentration.

Before each study, the reproducibility of the ablation conditions was controlled by measuring of a reference intensity for copper metal. For solid samples (glasses and minerals), shot-to-shot repeatability of emission line absolute intensities is ~10%: the variability is due mainly to laser energy fluctuations. These values are in agreement with those reported by Geertsen et al. (1996). The noise of the electronic detection system limits the repeatability to ~3%. So the reproducibility of this technique is close to that obtained with the electron microprobe for analyses of solid matrixes.

The emission line selected for lithium analysis is the most intense line, but it is also a resonance line (Weast, 1980). The use of a resonance line implies problems due to the potential for self-absorption (Autin, 1990). This is caused by reabsorption of the emitted photons by atoms in their fundamental electronic level and located in the colder external part of the plasma, reducing the overall emission intensities. Because the spectral resolution of the spectrometer is not sufficient, self-absorption is indicated by nonlinearity of the calibration curve (Fig. 1) and a decreasing slope with increasing concentration. Extrapolation

Table 1. Compositions (in wt%) of the synthetic glasses used to establish the lithium calibration curve. (ND = not determined).

SG	SiO_2	Al_2O_3	Na_2O	K_2O	CaO	Li_2O
SG1	ND	ND	ND	ND	ND	0.002
SG2	ND	ND	ND	ND	ND	0.005
SG3	ND	ND	ND	ND	ND	0.009
SG4	ND	ND	ND	ND	ND	0.011
SG5	ND	ND	ND	ND	ND	0.021
SG6	73.04	15.32	3.85	4.96	0.85	0.037
SG7	72.94	15.57	4.56	4.14	0.57	0.08
SG8	ND	ND	ND	ND	ND	0.10
SG9	50.00	14.00	5.50	0.20	7.20	0.17
SG10	ND	ND	ND	ND	ND	0.18
SG11	ND	ND	ND	ND	ND	0.21
SG12	50.00	14.00	5.00	0.20	7.20	2.09
SG13	ND	ND	ND	ND	ND	3.30
SG14	62.64	17.44	1.19	10.87	4.68	4.13
SG15	58.05	15.73	10.06	—	—	18.54
SG16	81.98	7.42	0.15	—	0.07	13.16

Table 2. Compositions (in wt%) of micas used to establish the calibration curve for lithium concentration. (ND = not determined).

Element	Lepidolite	Muscovite
SiO_2	50.3	45.73
Al_2O_3	25.74	34.89
FeO(tot)	0	2.45
Fe_2O_3(tot)	—	—
MnO	0.4	0.02
MgO	0	0.48
CaO	0	0
Na_2O	0.32	0.48
K_2O	9.94	10
TiO_2	0	0.05
P_2O_5	ND	ND
B_2O_3	ND	ND
F	7.36	0.19
H_2Otot	ND	ND
Rb_2O	ND	—
Li_2O	5.62	0.23
Sum	99.66	94.52
Formula	$[Si_3AlO_{10}\|F_2]KLi_{1.5}Al_{1.5}$	$[Si_3AlO_{10}\|(OH)_2]KAl_2$

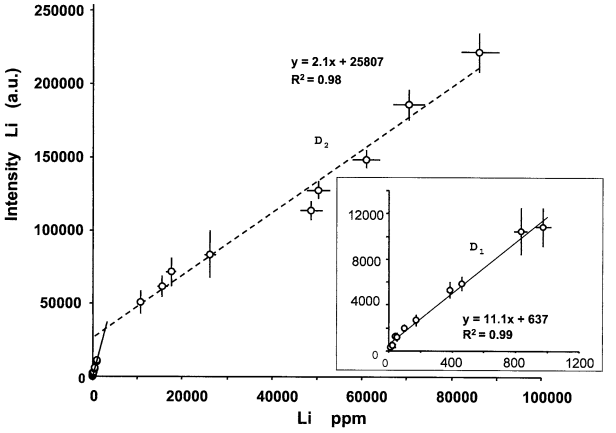

Fig. 1. Calibration of the lithium emission line at 670.7 nm. An expansion for values <1000 ppm is also represented (modified from Fabre et al., 1999).

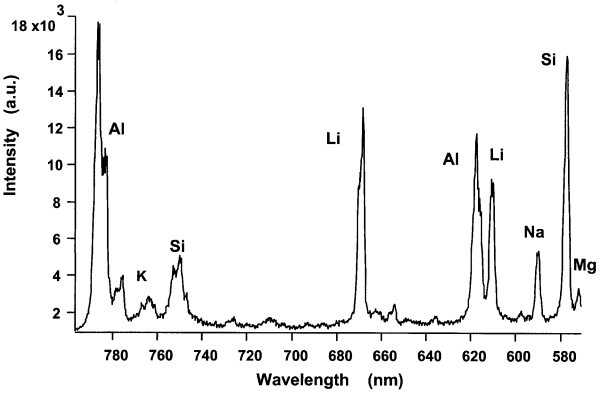

Fig. 2. Optical emission spectrum obtained after one laser shot in eucryptite, showing characteristic lines of aluminium, silicon, sodium, and lithium. Concentration of lithium is ~5000 ppm.

of the calibration curve, established for the highest concentrations, does not go through the origin. The calibration curve consists out of two branches, D_1 below ~3000 ppm Li, where self-absorption is negligible, and D_2 above this value. For LIBS analysis of either silicate glasses or liquids, the matrix effect is limited (Fabre et al., 1999). The detection limit, estimated for an optimal signal/noise ratio of 5, is ~5 ppm Li (emission line at 670.706 nm).

4. APPLICATIONS

4.1. Li-Rich Minerals

Lithium is often an important element in highly fractionated granitic environments (rare-element pegmatites), mainly forming phosphate minerals, silicate minerals, or both (London and Burt, 1982). Thus, the first application concerns Li-rich minerals such as spodumene ($LiAlSi_2O_6$), petalite ($LiAlSi_4O_{10}$), or eucryptite ($LiAlSiO_4$), which cohabit in some aplo-pegmatite dikes from Portugal (Charoy et al., 1995, 2001). Li concentration in petalite was determined by ion microprobe; spodumene compositions were obtained by wet chemistry on mineral separates and confirmed by ion microprobe analysis (CRPG). No data for lithium concentrations were available for the eucryptite mineral, which was positively identified by its fluorescence in short-wave ultraviolet light and Si/Al stoichiometry from punctual energy-dispersive spectrometry analysis. Eucryptite was intimately mixed with platy quartz, secondary albite, and K-feldspar, and with various phosphate phases.

The Li_2O concentrations for three spodumene grains is 7.6 ± 1.6 wt%, which is in excellent agreement with ion microprobe data (7.45 ± 0.5 wt%) and the bulk analysis of separated crystals (7.65 ± 0.3 wt%). The Li content of petalite determined by LIBS is ~6.3 ± 1.3 wt%, which is rather close to 4.49 ± 0.2 wt% measured by ion microprobe.

Analysis of eucryptite minerals was performed on three samples. In the first sample, Li concentrations vary from 50 to 1500 ppm and from 300 to 2800 ppm in the second one, whereas the third sample (Fig. 2) presents the highest Li concentration up to 6500 ppm (1.4 wt% of Li_2O). All of these values are far lower than theoretical eucryptite Li_2O value of 11.8 wt%. This is probably a result of the small size (<3 μm) of the eucryptite crystals and their intimate growth with other phases. Alkaline elements (potassium, sodium, and magnesium) were also detected (Fig. 2), suggesting the ablation of other minerals than eucryptite.

4.2. Glass and Daughter Minerals in Melt Inclusions from Streltsovka Uranium Deposit (Transbaikalia)

Numerous studies have been performed on melt inclusions in magmatic rocks to understand the geochemistry of magmas from which the inclusions are derived and to quantify variations in the magma chemistry during crystallization (Roedder, 1979; Clocchiatti, 1975; Clocchiatti and Krasov, 1979; Taylor et al., 1997; Webster and Duffield, 1991; Webster et al., 1997; Michaud et al., 2000). Growing crystals, particularly in a near-surface environment, tend to trap small globules of magma because of the breakdown of planar crystal–melt interfaces or because of defects in the growing crystal. Quartz, unlike feldspars, provides a well-sealed medium.

The Streltsovka caldera located in Transbaikalia close to the Chinese–Mongolian border is well known for its U-Mo deposits, which represent the largest uranium field in the world associated with volcanism. Chabiron (1999) and Chabiron et al. (2001) have already performed significant work on the Streltsovka uranium deposit. These studies focused on the geochemistry of the Streltsovka rhyolitic melt, which was based on an extensive study of melt inclusions trapped in quartz phenocrysts of the Streltsovka rhyolite.

The typical size of melt inclusions observed in quartz phenocrysts of the Streltsovka rhyolite ranges from 10 to 250 μm (Fig. 3). Platy minerals are commonly embedded in the largest melt inclusions. These crystals are presumably daughter minerals because (1) they are present constantly from one melt inclusion to the next; (2) in heating studies, these crystals dissolved before complete homogenization of the melt inclusions; and (3) there is a correlation between the volume of melt (glass) and the volume of crystals. Chabiron (1999) used optical microscopy, scanning electron microscopy, Raman spectroscopy, and electron microprobe to analyze these daughter

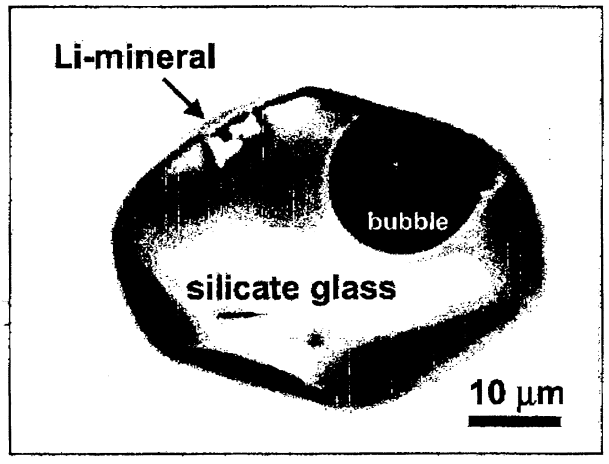

Fig. 3. Photomicrograph of the melt inclusion 1 mol/L1 displaying daughter minerals in silicate glass phase.

minerals. However, their small average size (~10 μm) limited the effectiveness of these techniques (Chabiron et al., 2001). F-rich micas were identified in melt inclusion, and their compositions vary from zinnwaldite to polylithionite. By use of the empirical relation $LiO_2 = 0.287 \times SiO_2 - 9.552$ (Tindle and Webb, 1990), LiO_2 content is estimated in the range of 2.2 to 5.1 wt% (Table 3). Tests were performed via LIBS on daughter minerals and glass in a number of melt inclusions to confirm the presence of lithium in such mica.

Two melt inclusions from samples 1 and 2 were analyzed (Table 3), both displaying 8-μm-long daughter minerals (Fig. 3). An optical emission spectrum obtained after one laser shot on the daughter mineral from melt inclusion shows that Li is present (Fig. 4A). Li_2O concentrations by LIBS for the two daughter minerals are 2.1 ± 0.3 wt% and 1.9 ± 0.2 wt%, respectively; this is in good agreement with data deduced from the empirical formula (Tindle and Webb, 1990; Tischendorf et al., 1997) for the same minerals via electron microprobe analysis (2.2 ± 0.2 wt%; Table 3). Moreover, the Na/K ratio for the mica was found to be ~0.03 ± 0.006% by using LIBS, in relative agreement with the electron microprobe estimation of 0.05 obtained on the same Li-rich mica (2 mol/L1). This result is acceptable because the shot number is rather low (five data). The lithium concentrations are estimated ~90 ± 20 ppm and 180 ± 50 ppm, respectively, for the two silicate glasses (Fig. 4B).

Two lithium concentrations were also estimated for sample 3 on two melt inclusions not previously studied by electron microprobe (no data available). Their Li-rich daughter minerals display Li_2O concentrations of 4 and 6.2 wt%. Separate analyses of Li_2O deduced from electron microprobe data on different daughter minerals from the same sample range from 3.6 to 5.1 wt% (Table 3)—results in relatively good agreement with those obtained via LIBS. For these melt inclusions, Li content in silicate glasses is ~300 ppm. This study shows that Li quantification is possible by using the LIBS technique both in glass and associated daughter minerals in melt inclusions.

4.3. Hydrothermal Quartz: Correlation between Lithium Content and Cathodoluminescence

The observations by cathodoluminescence (CL) of hydrothermal and diagenetic quartz reveal zones of varying intensity and wavelength of the CL emission. The factors responsible for CL properties in quartz, generally thought to be related to the presence of trace elements during crystal growth, are still debated (Remond, 1977; Watt et al., 1997; Perny et al., 1992; Remond et al., 1992). Quantitative in situ trace element determinations (generally in quartz) can be obtained via the ion microprobe (Shimizu et al., 1978; Perny et al., 1992). More recently, an integrated study (ion microprobe and CL images) on detrital quartz in sandstones from the French Paris Basin

Table 3. Composition of Li-rich daughter minerals from several melt inclusions from the Streltsovka deposit obtained by electron microprobe. Estimated lithium concentrations are obtained from electron microprobe (deduced from the empirical formula) and the LIBS technique[a]

Melt inclusion	1-M1[a]	1-M2	2-M1[a]	3-M1	3-M2	3-M3	3-M4
SiO_2	40.8	41.3	41.0	47.6	45.8	51.0	48.5
TiO_2	0.5	0.8	0.8	0.95	0.4	0.2	1.1
Al_2O_3	10.0	11.5	11.3	18.4	25.9	30.1	19.8
FeO	21.1	19.6	22.2	15.1	8.4	2.3	7.3
MnO	2.9	1.4	2.6	0.94	1.1	0.4	1.0
MgO	3.7	2.1	2.0	0.68	—	—	—
CaO	—	—	—	—	—	—	0.6
Na_2O	0.5	0.6	0.6	0.4	0.6	1.1	0.3
K_2O	9.5	10.4	10.3	10.3	10.3	8.8	10.5
F	6.1	5.3	5.2	5.7	6.8	5.7	8.5
Total	95.1	93.0	96.0	100.1	99.3	99.5	97.0
O=F	2.6	2.2	2.2	2.4	2.9	2.4	3.6
Total	92.5	90.8	93.8	97.7	96.4	97.1	93.5
Li_2O^a	2.2	2.3	2.2	4.1	3.6	5.1	4.4
Total	94.7	93.1	96.0	101.8	100.0	102.2	97.8
Li_2O^{LIBS}	2.2	ND	1.9		4 and 6.2		
Li^{LIBS}	90	ND	180		330		

[a] The same melt inclusions have been analyzed by LIBS and electron microprobe. Li_2O^a is the electron microprobe estimation on daughter mineral (wt%). Li_2O^{LIBS} is LIBS estimation on daughter mineral (wt%). Li^{LIBS} is LIBS estimation in silicate glass (ppm). (ND = not determined).

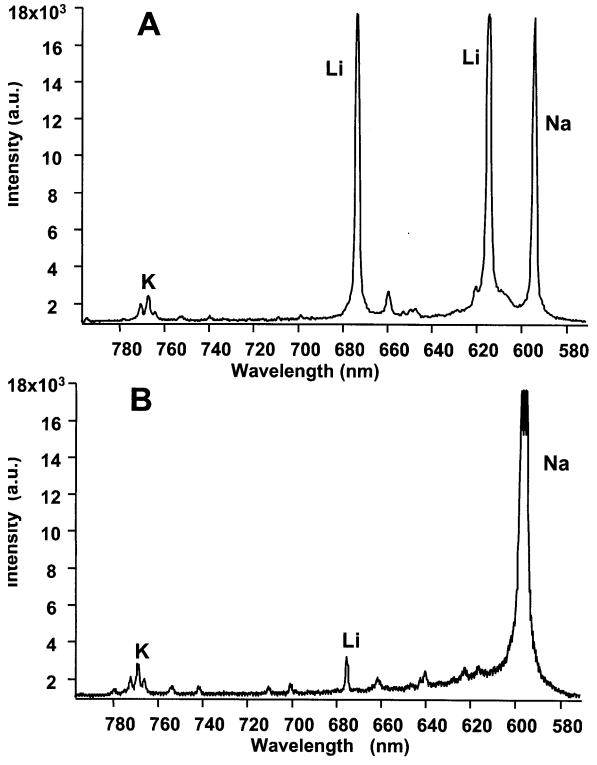

Fig. 4. Optical emission spectra obtained in a melt inclusion and its daughter mineral. A filter was used to limit the aluminium and silicon emissions. Characteristic emission lines of potassium, sodium, and lithium are labeled. (A) Optical emission spectrum obtained after one shot in the mica. The Li_2O content is ~2 wt%. (B) Optical emission spectrum obtained after one shot in the glass. Estimated of lithium content is ~100 ppm.

demonstrated that Li was present up to 30 ppm in quartz overgrowths (Demars et al., 1996) and was correlated with more intense CL emission.

Quartz from several barren hydrothermal veins from the Spanish Central System (Sierra de Guadarrama) show minute variations in the CL emission. LIBS analyses were performed along a profile cross-cutting the different CL zones to determine the variation of trace elements, especially to determine whether Li concentration correlates with CL.

Figure 5 shows changes in CL intensities that appear to be related to growth bands. The LIBS profile was achieved by making one laser shot, along the a–b section, every 50 μm. The sections studied were selected for their lack of fluid inclusions. The highest Li concentrations correlate with the brightest bands, and the values were found to be between 250 to 370 ppm. The darkest region observed in CL had the lowest Li amounts (Li $<$ 100 ppm; Fig. 5). Such a correlation was confirmed along other profiles where the brightest luminescence zones systematically display the highest Li concentrations obtained by the LIBS technique.

Fluid inclusions in the Sierra de Guadarrama quartz have been also studied (Martin Crespo et al., 1999). Two types of aqueous fluids were described: low-salinity H_2O-NaCl fluids, and high-salinity H_2O-$CaCl_2$-NaCl fluids. These last high salinity brines display a low first melting temperature (−67 to −55°C), possibly suggesting the presence of Li (in addition to

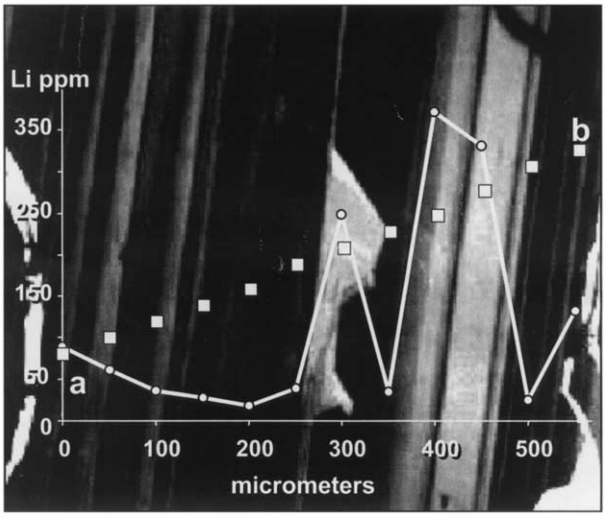

Fig. 5. Cathodoluminescence photomicrograph of hydrothermal quartz showing zonation of luminescence intensities. The a–b profile is shown by the squares. Each square corresponds to one laser shot and to one LIBS analysis. The Li estimates (ppm) are also reported.

calcium). LIBS analysis was performed on individual primary fluid inclusions, and the Na/Li molar ratio for the fluid was estimated to be between 3 and 14. Thus, the high Li content in the quartz growth zones could be the result of quartz precipitation from a Li-rich fluid, as found in fluid inclusions. These brines came from a sedimentary basin, where they could have interacted with evaporites, as suggested by the results of crush leach analyses of fluid inclusions (Martin Crespo et al., 1999). High Li values were reported for saline solutions from the Paris Basin (Fontes and Matray, 1993; Demars et al., 1996). The authors suggest that Li in high-salinity fluids is the result of diagenetic reactions within nearby sedimentary basins. Therefore, the Li-rich hydrothermal quartz analyzed could have precipitated from high-salinity fluids originating from a similar environment and percolating through the crystalline basement.

5. CONCLUSIONS

This study shows that lithium can be easily analyzed via LIBS in natural glasses and minerals. To estimate the lithium content of different geological materials, LIBS calibration was achieved by using synthetic glasses and natural minerals. The detection limit is ~5 ppm when the Li emission line at 670.706 nm is used. Compared with the electron microprobe technique, the LIBS technique offers a direct determination of lithium (rather than empirical calculation), with a lower detection limit (5 ppm Li) at a slightly poorer spatial resolution (6 to 8 μm). Three applications were performed to show the potential of LIBS for lithium analysis at the micrometric scale in geological materials.

First, the Li-rich minerals petalite and spodumene from granite pegmatite dikes (Portugal) have Li_2O concentrations of 7.6 ± 1.6 wt% and 6.3 ± 1.3 wt%, respectively. LIBS analyses are in good agreement with bulk and micropobe data obtained for the same minerals. In contrast, eucryptite analyses are inaccurate because of

their intimate mixture with other minerals at the micrometric scale, resulting in dilution of bulk Li concentration.

Second, quantification of the lithium content was performed on melt inclusions from the Streltsovka uranium deposits (Russia). Li_2O is in the range of 2 to 6.2 wt% for Li daughter minerals, and Li comprises between 90 and 400 ppm in the glass phases. These estimates are in agreement with those deduced from the empirical EPMA formula on platy minerals. LIBS analysis is thus of great interest for the characterization of the magma geochemistry and the determination of Li partitioning between minerals and melt, especially in the study of rare-metal deposits.

Third, profiles across hydrothermal quartz (Sierra de Guadarrama, Spain) permit the correlation of cathodoluminescence intensities and Li concentrations (from several parts per million to several hundreds parts per million of lithium). The highest Li concentrations (250 to 370 ppm) were found in the brightest growth bands. The Li enrichment in quartz is probably due to a highly saline fluid that originated from sedimentary basins, as suggested previously by a fluid inclusion study.

This advance in Li analysis by LIBS constitutes a new step in punctual determination of Li at a trace-element level in minerals. The LIBS technique has to be considered as a reliable analytical tool due its practical advantages: low detection limits, easy facilities for sample analysis, fast acquisition, and relatively low cost. The LIBS method can be also applied to the detection of another trace elements, such as Ti, Cs, Be, Sn, or Mo, in the melt inclusion study, or more particularly to Al or Na in quartz substitution.

Acknowledgments—We thank M. Chaussidon (CRPG, Nancy) for supplying the standard Li minerals. We thank Robert Burruss, Alan Kolker, and an anonymous reviewer for their helpful and thoughtful reviews, which greatly improved the manuscript.

*Associate editor:*R. C. Burruss

REFERENCES

André N. (1995) Etude de plasmas produits par laser à pression atmosphérique en vue de l'analyse élémentaire dans les solides. Ph.D. thesis, Paris University.

Autin M. (1990) Caractérisation par spectrométrie d'émission et de fluorescence d'un plasma produit par ablation laser à pression atmosphérique. Application à l'analyse élémentaire dans les solides. Ph.D. thesis, Lyon University.

Brock K. J. (1974) Zoned lithium–aluminium mica crystals from the Pala pegmatic district. *Am. Mineral.* **59,** 1242–1248.

Chabiron A. (1999) Les gisement d'uranium de la caldeira de Streltsovka (Transbaïkale, Russie). Ph.D. thesis, Nancy University.

Chabiron A., Alyoshin A. P., Cuney M., Deloule E., Golubev V. N., Velitchkin V. I., and Poty B. (2001) Geochemistry of the rhyolitic magmas of the Streltsovka caldera (Transbaikalia, Russia): A magmatic inclusion study. *Chem. Geol.* **175,** 273–290.

Charoy B., Chaussidon M., and Noronha F. (1995) Lithium zonation in white micas from the Argemela microgranite (central Portugal): An in situ ion-, electron-microprobe and spectroscopic investigation. *Eur. J. Mineral.* **7,** 335–352.

Charoy B., Noronha F., and Lima A. (2001) Spodumene–petalite–eucryptite: Mutual relationships and alteration style in Li-rich aplite–pegmatite dykes from northern Portugal. *Can. Mineral.* In press.

Clocchiatti R. (1975) Les inclusions vitreuses des cristaux de quartz. Etude thermo-optique et chimique. Applications géologiques. *Soc. Géol. Fr. Mém.* **122,** 96.

Clocchiatti R. and Krasov N. (1979) Cristallisation fractionnée et immiscibilité dans les liquides silicatés calco-alcalins piégés dans les phénocristaux de plagioclase des laves du volcan Karimski (Kamchatka, URSS). *C. R. Acad. Sci. Paris* **289,** 1–4.

Demars C., Pagel M., Deloule E., and Blanc P. (1996) Cathodoluminescence of quartz from sandstones: Interpretation of the UV range by determination of trace element distributions and fluid inclusion P-T-X properties in authigenic quartz. *Am. Mineral.* **81,** 891–901.

Fabre C. (2000) Reconstitution chimique des paléofluides par spectrométrie d'émission optique couplée à l'ablation laser: Applications aux fluides alpins et aux fluides de bassins. Ph.D. thesis, Nancy University.

Fabre C., Boiron M. C., Dubessy J., and Moissette A. (1999) Determination of ions in individual fluid inclusions by laser ablation–optical emission spectroscopy: Development and applications to natural fluid inclusions. *J. Anal. At. Spectrom.* **14,** 913–922.

Fabre C., Boiron M. C., Dubessy J., Cathelineau M., and Banks D. A. (2001) Paleofluid chemistry of single fluid event: A bulk and in situ multi-technique analysis (LIBS, Raman spectroscopy) of an alpine fluid (Mont Blanc). *Chem. Geol.*In press.

Fontes J. C. and Matray J. M. (1993) Geochemistry and origin of formation brines from Paris Basin, France. 1. Saline solutions associated with oil fields. *Chem. Geol.* **109,** 177–200.

Geertsen C., Lacour J. L., P. Mauchien P., and Pierrard L. (1996) Evaluation of laser ablation optical emission spectrometry for microanalysis in aluminium samples. *Spectrochim. Acta* **51,** 1403–1416.

Henley R. W., Truesdell A. H., and Barton P. B. Jr (1984) Fluid–mineral equilibria in hydrothermal systems. In *Reviews in Economic Geology*(eds. R. W. Henley, A. H. Truesdell, and P. B. Barton Jr), Vol. 1. Society of Economic Geologists.

London E. (1992) The application of experimental petrology to the genesis and crystallization of granitic pegmatites. *Can. Mineral.* **30,** 499–540.

London D. and Burt D. M. (1982) Lithium–aluminosilicate occurrences in pegmatites, and the lithium–aluminosilicate phase diagram. *Am. Mineral.* **67,** 483–493.

Martin Crespo T., Lopez Garcia J., Banks D., Vindel E., and Garcia E. (1999) Hydrothermal barren fluids in barren quartz veins (Spanish Central system): A comparison with W (Sn) and F (Ba) veins. *Bol. Soc. Esp. Mineral.* **22,** 83–94.

Mauchien P., Bengston A., DeMarco R., DaSilva E., Dubessy J., Noronha F., Prieto C., Tomandl G., and Yardley B. W. (1996) Study of emission spectroscopy on laser produced plasma for localised multielemental analysis in solids with surface imaging. In final report, European program "Measurement and Testing," MAT1-CT-93-0029.

Michaud V., Clocchiatti R., and Sbrana S. (2000) The Minoan and post-Minoan eruptions, Santorini (Greece), in the light of melt inclusions: Chlorine and sulphur behaviour. *J. Volcan. Geotherm. Res.* **99,** 195–214.

Moenke-Blankenburg L. (1989) Laser micro analysis. In *Chemical Analysis: A Series of Monographs on Analytical Chemistry and Its Applications*, 105. Wiley Interscience.

Perny B., Eberhardt P., Ramseyer K., Mullis J., and Pankrath R. (1992) Microdistribution of aluminium, lithium and sodium in α quartz: Possible causes and correlation with short-lived cathodoluminescence. *Am. Mineral.* **77,** 534–544.

Radziemski L. J. and Cremers D. A. (1989) *Laser Induced Plasma and Its Applications*. Marcel Dekker.

Remond G. (1977) Applications of cathodoluminescence in mineralogy. *J. Luminescence* **15,** 121–155.

Remond G., Cesbron F., Chapoulie R., Ohnenstetter D., Roques-Carmes C., and Schvoerer M. (1992) Cathodoluminescence applied to the microcharacterization of mineral materials: A present status in experimentation and interpretation. *Scanning Microscopy* **6,** 23–68.

Roedder E. (1979) Origin and significance of magmatic inclusions. *Bull. Mineral.* **102,** 487–510.

Seitz H. M. and Woodland A. B. (2000) The distribution of lithium in peridotic and pyroxenitic mantle lithologies—An indicator of magmatic and metasomatic processes. *Chem. Geol.* **166,** 47–64.

Shimizu N., Semet M. O., and Allègre C. (1978) Geochemical applications of quantitative ion microprobe analysis. *Geochim. Cosmochim. Acta* **42,** 1321–1334.

Stern L. A., Brown G. E., Bird D. K., Jahns R. H., Foord E. E., Shigley J. E., and Spaulding L. B. (1986) Mineralogy and geochemical evolution of the Little Three pegmatite–aplite layered intrusion, Ramona, California. *Am. Mineral.* **71,** 406–427.

Taylor R. P., Jackson S. E., Longerich H. P., and Webster J. D. (1997)

In situ trace element analysis in individual silicate melt inclusions by laser ablation microprobe–inductively coupled plasma–mass spectrometry (LAM-ICP-MS). *Geochim. Cosmochim. Acta* **61,** 2559–2567.

Tindle A. G. and Webb P. C. (1990) Estimation of lithium content in trioctahedral micas using microprobe data: Application to micas from granitic rocks. *Eur. J. Mineral.* **2,** 595–615.

Tischendorf G., Gottesmann B., Forster H. J., and Trumbull R. B. (1997) On Li-bearing micas: Estimating Li from electron microprobe analyses and an improved diagram for graphical representation. *Mineral. Mag.* **61,** 809–834.

Watt G. R., Wright P., Galloway S., and McLean C. (1997) Cathodoluminescence and trace element zoning in quartz phenocrysts and xenocrysts. *Geochim. Cosmochim. Acta* **61,** 4337–4348.

Weast R. C. (1980) *Handbook of Chemistry and Physics.* CRC Press.

Webster J. D. and Duffield W. A. (1991) Volatile and lithophile elements in Taylor Creek Rhyolite: Constraints from glass analysis. *Am. Mineralogist.* **76,** 1628–1645.

Webster J. D., Thomas R., Rhede D., Förster H. J., and Stelmann R. (1997) Melt inclusions in quartz from an evolved peraluminous pegmatite: Geochemical evidence for strong tin enrichment in fluorine-rich and phosphorus-rich residual liquids. *Geochim. Cosmochim. Acta* **61,** 2589–2604.